Auroral ion acceleration in dispersive Alfvén waves

C. C. Chaston,[1] J. W. Bonnell,[1] C. W. Carlson,[1] J. P. McFadden,[1] R. E. Ergun,[2]
R. J. Strangeway,[3] and E. J. Lund[4]

Received 20 May 2003; revised 4 January 2004; accepted 9 February 2004; published 3 April 2004.

[1] Observations from the FAST satellite are used to create a model for dispersive Alfvén waves above the auroral oval. Using this model, it is shown how these waves may accelerate ionospheric ions transverse to the geomagnetic field and cause ion outflow. The model waves grow from ionospheric conductivity variations due to auroral electron precipitation and resonate in the cavity between the ionosphere and the peak in the Alfvén speed that occurs at altitudes of ~1 Earth radius (Re). By tracing ions in the model wave field, it is demonstrated that for transverse wave amplitudes ($E_\perp$) satisfying $E_\perp/B_o < \Omega_i/k_\perp$ (where B_o is the geomagnetic field strength, $k_\perp$ is the perpendicular wave number, and Ω_i is the ion gyrofrequency) the ion motion in the wave field is coherent and the ions may become trapped in the transverse wave potential. In Alfvén waves having two-dimensional structure transverse to B_o, these ions may be accelerated up to a transverse energy that provides an ion gyrodiameter roughly equivalent to the perpendicular scale or wavelength ($\lambda_\perp$) of the wave. Alternatively, when $E_\perp/B_o > \Omega_i/k_\perp$ the ion motion may become stochastic allowing acceleration to energies exceeding that prescribed by $\lambda_\perp$. The transversely accelerated ions in both the coherent and stochastic cases flow upward from the ionosphere under the influence of the mirror force to altitudes of 1 Earth radii over timescales as small as a few seconds to minutes with energies in the keV range. Ions accelerated by these means may account for the intense outflowing ion fluxes observed in Alfvén waves above the auroral oval. *INDEX TERMS:* 2732 Magnetospheric Physics: Magnetosphere interactions with satellites and rings; 2704 Magnetospheric Physics: Auroral phenomena (2407); 2451 Ionosphere: Particle acceleration; 2431 Ionosphere: Ionosphere/magnetosphere interactions (2736); 2483 Ionosphere: Wave/particle interactions; *KEYWORDS:* ion heating, ion acceleration, Alfvén waves, kinetic effects, aurora, ionospheric Alfvén resonator

Citation: Chaston, C. C., J. W. Bonnell, C. W. Carlson, J. P. McFadden, R. E. Ergun, R. J. Strangeway, and E. J. Lund (2004), Auroral ion acceleration in dispersive Alfvén waves, *J. Geophys. Res.*, *109*, A04205, doi:10.1029/2003JA010053.

1. Introduction

[2] There are many mechanisms suggested for the acceleration of ions in the magnetosphere [*Andre and Yau*, 1997]. Above the auroral ionosphere the most relevant mechanisms include acceleration in parallel to the geomagnetic field ($\mathbf{B}_o$), quasi-static electrostatic potentials, and transverse acceleration in waves driven by electron and ion currents or beams [*Hultqvist et al.*, 1999]. For self-consistency, however, these mechanisms require the presence of a parallel to $\mathbf{B}_o$ potential drop at some altitude above the auroral oval or at least field-aligned currents. In the case of electrostatic ion acceleration this requirement is obvious. However, for the wave-heating mechanisms it is required to provide the currents and/or the ion and electron beams necessary to excite instabilities. These drive the necessary wave modes to heat the ions through cyclotron resonance. In the cusps and polar cap boundary, inverted-V electrons are usually not present, and it is difficult to identify a distinct current direction. Consequently, in these regions the usual mechanisms are unable to self-consistently account for ion acceleration due to the absence of an energy source for the ion waves. Alfvén waves however, are a nearly permanent feature in these regions [*Chaston et al.*, 2003a]. It is possible that these waves may stimulate instabilities to generate waves at frequency approaching the ion gyrofrequency [*Lysak and Carlson*, 1981; *Penano and Ganguli*, 2000; *Wu and Seyler*, 2003; *Genot et al.*, 2004] or may directly accelerate the ions to account for the observations [*Knudsen and Wahlund*, 1998; *Stasiewicz et al.*, 2000a]. The second possibility is investigated in this report.

[3] There are at least two possible mechanisms by which Alfvén waves with frequency $\omega \ll \Omega_i$ may accelerate ions. In the case where the perpendicular wave number is much less than the inverse ion gyroradius (i.e., $k_\perp \ll 2\pi/\rho_i$), a possible acceleration process is due to the ponderomotive

[1]Space Sciences Laboratory, University of California, Berkeley, California, USA.
[2]Laboratory for Atmospheric and Terrestrial Physics, University of Colorado, Boulder, Colorado, USA.
[3]Institute for Geophysical and Planetary Physics, University of California, Los Angeles, California, USA.
[4]Space Science Center, University of New Hampshire, Durham, New Hampshire, USA.

0148-0227/04/2003JA010053$09.00

force. This was first postulated for the aurora by *Li and Temerin* [1993]. In this mechanism the force experienced by the ions is proportional to, and in the direction of, the gradient along $\mathbf{B}_o$ in the square of the perpendicular wave electric field ($E_\perp$). The resulting force is upward and out of the auroral oval where positive gradients in $E_\perp$ with altitude exist. This is usually the case at low altitudes (<1 Re) because the altitude dependency of the Alfvén speed here provides increasing perpendicular electric field amplitudes with altitude. The exception is where nodes in $E_\perp$ occur due to harmonics of the ionospheric Alfvén resonator [*Lysak*, 1991]. This means of ion acceleration has been shown to provide fluxes of low energy ions reaching altitudes of the order of 1 Re from the upper ionosphere over periods of ~10 min [*Li and Temerin*, 1993].

[4] The second mechanism, which is the topic of this report, involves the comparatively rapid acceleration experienced by an ion as it travels through the perpendicular wave field of an obliquely propagating wave where $k_\perp \sim 2\pi/\rho_i$. For sufficiently large $E_\perp/B_o$ the particle motion may become stochastic. This process, in the terrestrial magnetosphere, has been studied in some detail by *Reitzel and Morales* [1996] and *Ram et al.* [1998] for lower hybrid waves, by *Lysak et al.* [1980] and *Papadopoulos et al.* [1980] for electrostatic ion cyclotron waves, and by *Stasiewicz et al.* [2000a] and *Johnson and Cheng* [2001] as a means for energizing ions in Alfvén waves. In this mechanism the ion acceleration is in the transverse direction and operates most effectively when $k_\perp$ is a significant fraction of $2\pi/\rho_i$ or, in a more basic sense, when a particle gyrates or travels through large changes $E_\perp$ [*Cole*, 1976]. The disruption of the ion orbit that occurs in this case is similar to that caused by motion through a narrow oblique auroral double layer as studied previously by *Borovsky* [1984] and *Greenspan* [1984]. In small-scale Alfvén waves, ion outflow is provided by the mirror force acting on the ions' enhanced magnetic moment that the orbit disruption provides.

[5] Theories for ion acceleration in a single coherent, large-amplitude, transverse electrostatic wave have been developed by *Karney and Bers* [1977], *Karney* [1978], *Lysak et al.* [1980], *Lysak* [1986a], and *Chen et al.* [2001]. These theories indicate that for a plane monochromatic wave with $k_\perp\rho_i > \omega/\Omega_i$ (or $v_\perp > v_{phase}$) and $\omega/\Omega_i > 0$, the ion motion in the wave field may become stochastic if the displacement of the ion guiding center due to polarization drift over one wave period is similar to, or greater than, the perpendicular wavelength of the wave. This threshold can be written in terms of the wave amplitude as

$$E_\perp/B_0 = \alpha(\omega).\Omega_i/k_\perp, \quad (1)$$

where α is a frequency dependent quantity. This is the condition employed by *Stasiewicz et al.* [2000a] in explaining ion heating seen in similar waves observed from the Freja spacecraft. This result is independent of the wave mode involved except in the requirement that $B_o \gg B_{\perp 1,2}$. The subscripts 1 and 2 indicate the two orthogonal components transverse to B_o or the 3 direction. For Alfvén waves above the aurora, $B_{\perp 1,2}$ is several orders of magnitude smaller than B_o, and so it is reasonable to assume that the threshold given by equation (1) applies to Alfvén waves in this region. The frequency dependence of this threshold condition has been estimated numerically. *Karney and Bers* [1977] have shown for waves with $\omega \gg \Omega_i$ that $\alpha(\omega) = 1/4(\omega/\Omega_i)^{2/3}$. *Chen et al.* [2001] show, for waves with $\omega < \Omega_i$, that α increases with decreasing frequency and is close to 1. The addition of multiple waves to the system has been shown by *Lysak et al.* [1980] to lower the minimum wave amplitude required for stochastic motion. Once the minimum threshold has been exceeded, the maximum energy that an ion can gain from the wave is determined by an upper limit on the gyroradii for stochastic ion motion. *Karney* [1978] has shown this limit to be given by

$$E_\perp/B_0 = \eta(\omega)(\rho_i k_\perp)^{\frac{3}{2}}.\Omega_i/k_\perp, \quad (2)$$

with $\eta(\omega) = 1/4(\Omega_i/\omega)\ (\pi/2)^{0.5}$ for waves satisfying $\omega \gg \Omega_i$. A similar limit has been derived by *Lysak* [1986a] for the cyclotron resonant case ($\omega = n\Omega_i$). To our knowledge, however, no studies to determine this limit for the case where $\omega < \Omega_i$ have been performed.

[6] Outside the range of wave amplitudes specified by these thresholds, the ion motion is coherent. For sufficiently large wave amplitudes the ion becomes trapped and oscillates in the wave potential. For coherent ion motion in the cyclotron resonant case *Lysak et al.* [1980] have shown analytically that the energy of the accelerated ion, which becomes trapped in the wave potential, is limited by the perpendicular scale of the wave. For the fundamental resonance, this restriction requires $k_\perp\rho_i \sim < 3.8$ (or roughly $\rho_i \sim < \lambda_\perp/2$) but may be higher in the case of multiple waves. A similar result has been obtained numerically in electromagnetic ion cyclotron waves by *Chaston et al.* [2002a] and demonstrated to limit the energy of accelerated ions from FAST.

[7] In this report we show how ions may be accelerated in the Alfvén waves observed from the FAST spacecraft. We begin in section 2 by showing a case study example of the simultaneous observation of accelerated ions and Alfvén waves. We then determine the properties of these waves in section 3 and provide an empirically based altitude dependent model for the plasma above the auroral oval in section 4. In section 5 we use the observations to develop a model for the Alfvén waves above the aurora including electron inertial and ion kinetic effects for wave fields assumed periodic in directions transverse to B_o. In section 6, ions are injected into the model wave field and their trajectories traced to determine if Alfvén waves may cause ion outflow. Finally, in section 7 we summarize our findings and conclude.

2. Observations

[8] Figure 1 shows data collected during a traversal of the FAST spacecraft through the polar cap boundary of the auroral oval premidnight. Figure 1a shows the wave electric field ($\mathbf{E}_{\perp 1}$) measured perpendicular to the geomagnetic field ($\mathbf{B}_o$) and roughly in the North-South direction. Figure 1b is the magnetic field ($\mathbf{B}_{\perp 2}$) from the fluxgate magnetometer instrument measured perpendicular to $\mathbf{E}_{\perp 1}$ and perpendicular to $\mathbf{B}_o$ and roughly in the East-West direction. The red curves superimposed on this panel show high-resolution magnetic field data at frequencies above 1 Hz measured by

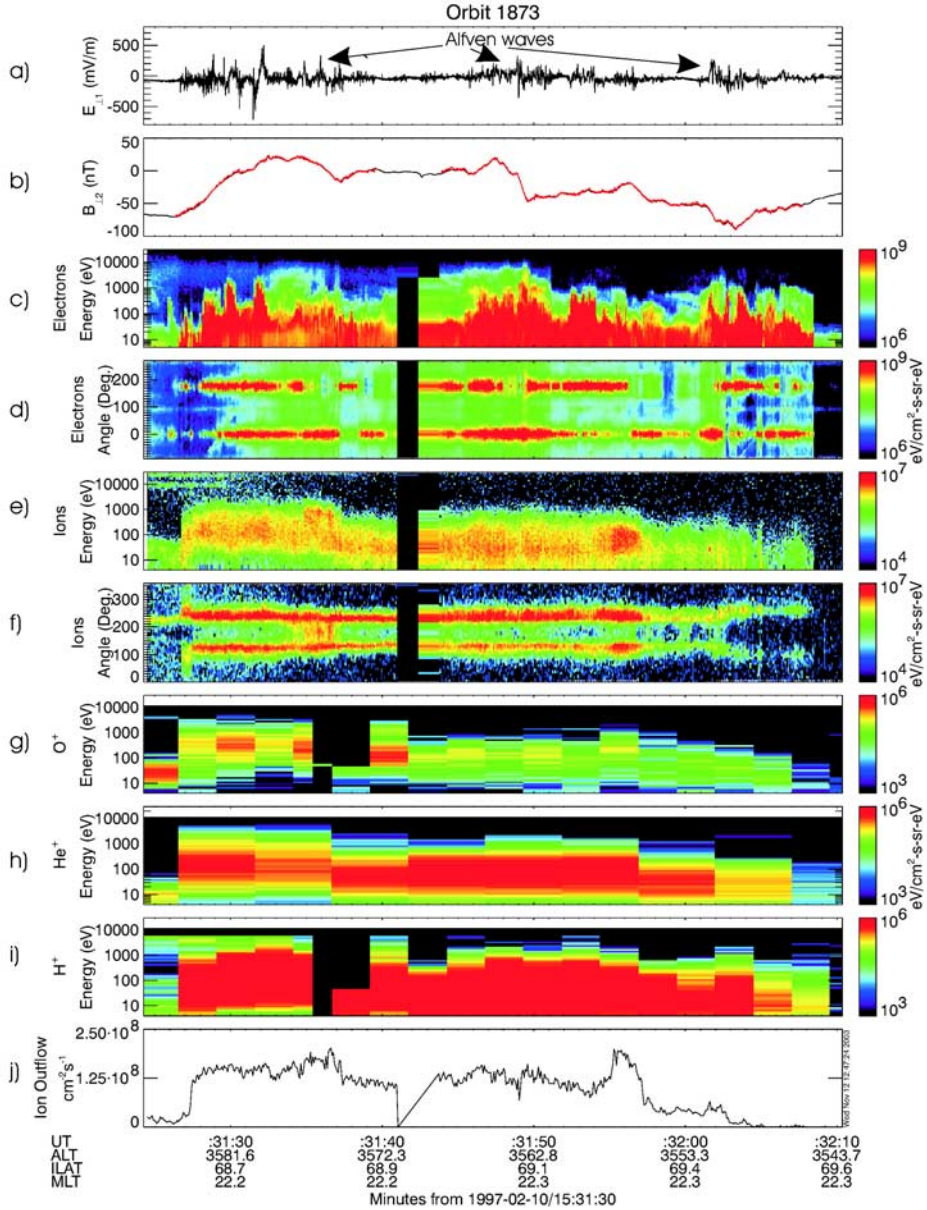

Figure 1. Observations from FAST on the polar cap boundary. (a) The electric field along the spacecraft trajectory or roughly north-south ($E_{\perp}1$). (b) The magnetic field measured transverse to the spacecraft trajectory and Bo, pointing roughly east-west ($B_{\perp 2}$). The red lines show high-resolution search coil data. (c) The energetic electron spectra. (d) The energetic electron pitch-angle spectra with 0^{o} pointing downward. (e) The ion energy spectra. (f) The ion pitch-angle spectra with 90 and 270^{o} pointing transverse to Bo. (g)–(i) The O^{+}, He^{+}, and H^{+} ion energy spectra and (j) the total integrated outflowing ion flux.

FAST's search coil magnetometer. The fluctuations in $\mathbf{E}_{\perp 1}$ and $\mathbf{B}_{\perp 2}$ observed throughout this interval have peak amplitudes up to a few 100 mV/m and tens of nT and cover a range of frequencies in the spacecraft frame extending well above the local oxygen gyrofrequency ($\Omega_{O+} = 14 \times 2\pi s^{-1}$ at this altitude). At frequencies below Ω_{O+} these fluctuations satisfy $E_{\perp 1}/B_{\perp 2} \approx 10^{7}$ $ms^{-1} \sim V_A$, which is the local Alfvén speed averaged over the interval displayed. This is shown in Figure 2b where we plot the ratio of the Fourier amplitudes as a function of frequency normalized by V_A.

[9] Figures 1c and 1d show the electron energy and pitch angle spectra. These reveal bursty field-aligned (0°) and counter field-aligned (180°) electron fluxes over the interval of enhanced wave activity. The field-aligned electrons fall within the source cone of electrons reaching the ionosphere and will cause aurora. Such observations are common in the presence of Alfvén waves above the auroral oval [*Stasiewicz et al.*, 2000b].

[10] The remaining panels show enhanced fluxes of energized ionospheric ions. The width of the region where enhanced ion fluxes are observed spans the region where

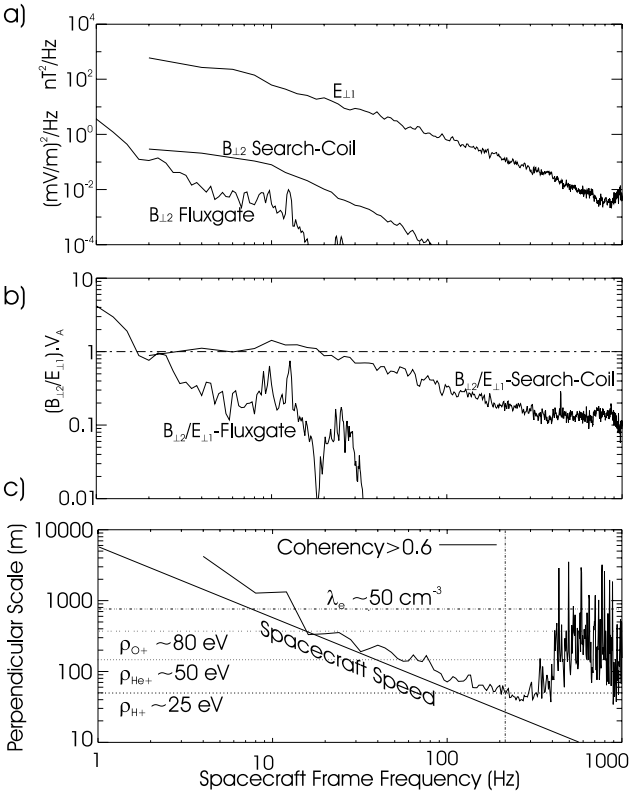

Figure 2. Spectral properties of low frequency waves on the polar cap boundary. (a) The wave power spectra averaged over the interval displayed in Figures 1a and 1b, including spectral results from the search coil magnetometer. (b) The $B_\perp 2/E_{\perp 1}$ ratio normalized by the local Alfvén speed of $\sim 10^7$ ms^{-1} from measurements using in one case the fluxgate magnetometer and in the other the search coil magnetometer. (c) The relationship between the perpendicular scale of the wave and the wave frequency in the spacecraft frame derived from a cross-spectral analysis as described in the text. The dot-dashed line is the trend expected for stationary structures subject to spacecraft Doppler shift. The dashed vertical line at ~200 Hz is the boundary between results where the two point coherency is >0.6 and incoherent signals. The horizontal lines are the electron inertial length (λ_e), the oxygen gyroradius (ρ_{O+}), the helium gyroradius (ρ_{He+}), and the hydrogen gyroradius (ρ_{H+}) derived from the observed density and temperatures.

the Alfvén waves are observed. Figure 1e shows that the energy of these ions extends just above 1 keV, while Figure 1f shows that the ion energy flux peaks at pitch angles close to 90° and 270°. This is indicative of local transverse acceleration. Figures 1g to 1i show that the energy fluxes and energies observed in each species are strongly mass dependent. H^+ ions supply the largest energy fluxes over energies extending from the lowest measured up to 1 keV. O^+ ions supply the smallest fluxes but on average are the most energetic, with the majority of the energy flux in this species above an energy of 100 eV. He^+ ions, in flux and energy, are intermediate between the H^+ and O^+ ions. The mass dependency of ionospheric ion acceleration and outflowing ion fluxes above the auroral oval has been discussed previously by numerous authors [*Andre and Yau*, 1997]. The specific case of increasing ion energy with mass, as observed here, has been identified in observations from a number of spacecraft [*Collin and Johnson*, 1985; *Knudsen et al.*, 1994; *Norqvist et al.*, 1996; *Lund et al.*, 2000]. The ion species included Figure 1 together provide very large total outflow fluxes as shown in Figure 1j. In fact they are amongst the largest seen in the nightside auroral oval and when integrated over the source region can account for a significant fraction of the ion density in the plasma sheet [*Tung et al.*, 2001].

3. Wave Properties

[11] Figure 2 shows the spectral properties of the waves shown in Figure 1 as a function of frequency in the spacecraft frame. The wave power spectra for the electric and magnetic field data, averaged over the interval of Figure 1, is displayed in Figure 2a. Here, results from both the fluxgate and search coil magnetometers are shown. The recursive filter on the fluxgate magnetometer limits measurements to waves below ~2 Hz for the operating mode of the instrument at this time. Above this frequency the search-coil magnetometer provides coverage as the fluxgate measurements roll off. Figure 2b contains the $B_\perp 2/E_{\perp 1}$.VA spectrum derived from Figure 2a. This result indicates that the observed fluctuations, over the frequency range from 2 to 20 Hz in the spacecraft frame, can be interpreted as Alfvén waves. Waves at higher frequencies become increasingly more electrostatic than the ideal Alfvén speed. These may still be interpreted as Alfvénic due to the electron inertial correction to Alfvén wave dispersion as demonstrated using Freja data by *Stasiewicz et al.* [2000c]. Importantly, this correction to the ideal MHD description is dependent on the perpendicular wave number, which can be estimated using interferometric techniques.

[12] A complete description of the interferometric analysis of these waves from FAST and the possible identification of these waves as Alfvénic can be found in the work of J. W. Bonnell et al. (An analysis of broadband ELF activity associated with ion conic outflows in the nightside polar cap boundary region, submitted to *Journal of Geophysical Research*, 2004, hereinafter referred to as Bonnell et al., submitted manuscript, 2004). We use this technique here to identify the perpendicular scales or wave numbers and frequencies appropriate for the simulations to follow. With this in mind, Figure 2c shows the results from a cross-spectral analysis using electric field measurements from two electric field dipoles on FAST. At the time when the data was recorded, the 11.5 m baseline between the two dipoles was perpendicular to $\mathbf{B}_o$. The result in Figure 2c shows perpendicular scales extending from 10,000 m down to tens of meters over the frequency range in the spacecraft frame from 0 to 200 Hz. Over this frequency range the coherence between the dipole measurements is greater than 0.6, indicating that the signals measured by each are related. The range of scales identified spans the gyroradii of the ion species present and also the electron inertial length. Since the direction of $k_\perp$ is not known, these scales cannot be identified as the $\lambda_\perp$ of the waves, but in the plane wave approximation they do represent a maximum possible $\lambda_\perp$ at each frequency.

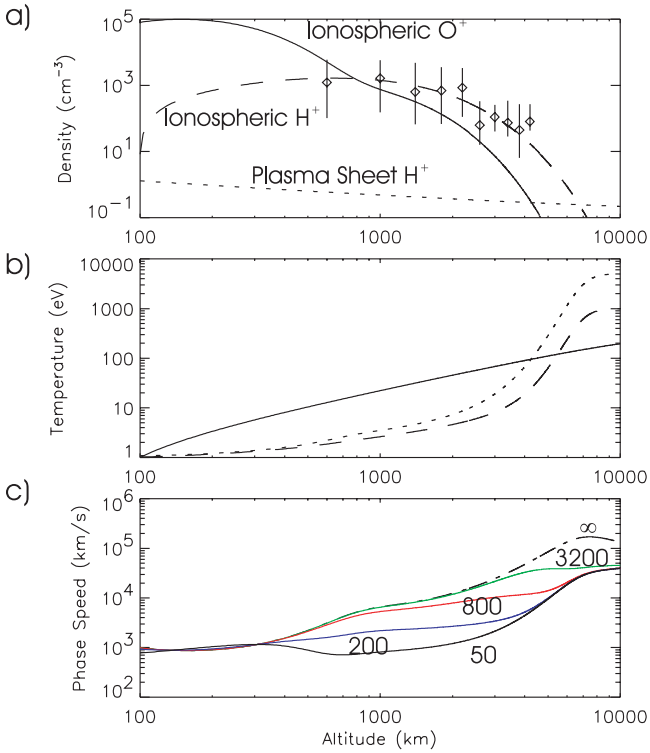

Figure 3. Altitude dependent model for energetic plasmas above the polar cap boundary. (a) The density of O_+ ions of ionospheric origin (solid line), H_+ ions of ionospheric origin (dashed line), and plasma sheet H_+ ions (dotted line). The diamonds show median measurements of the total density from FAST observations derived from the electron plasma line in altitude bins of 400 km width. The error bars show the range of densities in each bin. (b) The temperatures of the same components as described in the text. (c) The wave phase speed for the scales to be used in the simulation determined from equation (7) using the densities and temperatures defined in Figures 3a and 3b. The labels correspond to the perpendicular wavelength in m for each case at the ionosphere ($\lambda_{\perp 1i}$).

[13] The diagonal dot-dashed line in Figure 2c is the expected relationship between the perpendicular scale and the apparent wave frequency due to Doppler shift in the spacecraft frame for structures which are stationary in the rest frame. The similarity of the observed relationship with the spacecraft Doppler shift suggests that much of the temporal structure in $E_\perp$ and $B_\perp$ observed in the spacecraft frame may be largely stationary as previously proposed by *Stasiewicz et al.* [2000c] and Bonnell et al. (submitted manuscript, 2004). Significantly, for the acceleration mechanism to be simulated here, this means that much of the temporal variation in the plasma frame is at frequencies less than Ω_{O+}. To illustrate this, if we subtract the spacecraft Doppler shift, we obtain a range of frequencies from 0 to 100 Hz in the rest frame with wave frequencies exceeding Ω_{O+} only at scales smaller than ~100 m. The transition to frequencies exceeding Ω_{O+} may be shifted to even smaller scales if we include the likely contribution of plasma convection, which can provide an additional Doppler shift in the spacecraft frame. Given this result, it seems reasonable to assume that $\omega < \Omega_{O+}$ for the scales to be used in the simulations to follow.

4. Plasma Model

[14] Figure 3 shows a plasma model along a geomagnetic field line extending from 100 km up to 10,000 km in altitude. The densities and temperatures shown in Figures 3a and 3b for each species have been set to fit the observations at 3560 km discussed above. However, they are also consistent with statistically determined density and composition profiles for the polar cap boundary near midnight determined from FAST observations. These are indicated by the diamonds [*Chaston et al.*, 2003b]. The error bars shown here indicate the range of densities observed at each altitude. The temperature of the oxygen components is modeled in altitude using the same form adopted by *Lysak and Lotko* [1996] where T_{O+} = 1 + 499tanh(altitude − 100.)/(2Re) in electron Volts which provides a temperature of 1 eV at 100 km, ~80 eV at 3560 km altitude (as observed), and ~500 eV at altitudes above ~5 Re. For H^+ ions and electrons the profiles are averaged based on the contribution from ionospheric and plasma sheet densities shown in Figure 3a. The ionospheric profiles are given by $T_{H+,e-}$ = 1 + 499tanh(altitude − 100.) × 0.4/(2Re), and the plasma sheet ion and electron temperatures are taken to be 5 keV and 1 keV, respectively, consistent with the observations of Figure 1. This provides the steep temperature gradient above 3000 km altitude where the contribution of the plasma sheet to the average temperature becomes increasingly important. He^+ ions are not explicitly included here, and their inclusion has little effect on the results to be discussed.

5. Wave Model

[15] The model describes dispersive Alfvén waves assumed periodic in the plane perpendicular to B_o with two independent orthogonal wave numbers $k_{\perp 1}$ and $k_{\perp 2}$. The wave fields are given by

$$\begin{aligned} E_{\perp 1}(x,y,z,t) &= -k_{\perp 1}\phi(z,t)\cos(k_{\perp 1}x)\cos(k_{\perp 2}y) \\ E_{\perp 2}(x,y,z,t) &= k_{\perp 2}\Phi(z,t)\sin(k_{\perp 1}x)\sin(k_{\perp 2}y) \\ B_{\perp 1}(x,y,z,t) &= k_{\perp 2}A_\parallel(z,t)\sin(k_{\perp 1}x)\sin(k_{\perp 2}y) \\ B_{\perp 2}(x,y,z,t) &= k_{\perp 1}A_\parallel(z,t)\cos(k_{\perp 1}x)\cos(k_{\perp 2}y) \end{aligned} \tag{3}$$

Here $A_\parallel$(z, t) and φ(z, t) are the wave vector and scalar potentials; X, y, and z are coordinates in the two transverse and field-aligned direction, respectively; and t is time. These waves become planar when $k_{\perp 1} \rightarrow 0$ or $k_{\perp 2} \rightarrow 0$. Conveniently, we find $\nabla_\perp = (ik_{\perp 1}, ik_{\perp 2})$ and $\nabla_\perp^2 = -(k_{\perp 1}^2 + k_{\perp 2}^2)$ for these wave fields, and so the model formulation remains similar to that for plane waves as given by *Thompson and Lysak* [1996] or by *Chaston et al.* [2003c] in the kinetic case. Consequently, $A_\parallel$(z, t) and φ(z, t) obey the model equations

$$\frac{V_A^2}{c^2+V_A^2}\left[1+k_\perp^2\rho_i^2\right]\frac{\partial A_\parallel}{\partial z}+\frac{1}{c}\frac{\partial \Phi}{\partial t}=0 \tag{4}$$

$$\frac{\left[1+k_\perp^2\lambda_e^2\right]}{c}\frac{\partial A_\parallel}{\partial}=-\frac{\partial\Phi}{\partial z}\left(1+\frac{k_\perp^2\rho_s^2}{1+k_\perp^2\rho_i^2}\right). \quad (5)$$

Here $k_\perp^2 = k_{\perp 1}^2 + k_{\perp 2}^2$, ρ_i is the ion gyroradius; ρ_s is the ion acoustic gyroradii given by v_s/Ω_i, with v_s being the ion acoustic speed; and λ_e is the electron inertial length given by c/ω_{pe}, with ω_{pe} being the electron plasma frequency. The field-aligned wave magnetic field is zero, which from Faraday's law requires $k_{\perp 1}/k_{\perp 2} = E_{\perp 1}/E_{\perp 2}$, and the field-aligned electric field is

$$E_\parallel = -\frac{1}{c}\frac{\partial A_\parallel}{\partial t}-\frac{\partial\phi}{\partial z}=\frac{1}{c}\frac{\partial A_\parallel}{\partial t} \cdot\left[\frac{\left(1+k_\perp^2\lambda_e^2\right)\left(1+k_\perp^2\rho_i^2\right)-\left(1+k_\perp^2\left(\rho_i^2+\rho_s^2\right)\right)}{1+k_\perp^2\left(\rho_i^2+\rho_s^2\right)}\right]. \quad (6)$$

[16] From equations (4) and (5) in the local approximation these waves obey the dispersion relation

$$\omega/k_\parallel = V_A\sqrt{\frac{1+k_\perp^2\left(\rho_i^2+\rho_s^2\right)}{1+k_\perp^2\lambda_e^2}}, \quad (7)$$

which describes the wave accurately in this model except on steep field-aligned gradients. Figure 3c shows the wave phase speeds based on this dispersion relation for the density and temperature profiles illustrated in Figures 3a and 3b. The phase speed of the ideal MHD Alfvén wave is given by the dot-dashed black line where the term under the radical in equation (7) has been set to 1. The phase speed of the dispersive Alfvén wave from equation (7) is indicated by the solid color lines. The $\lambda_\perp s$ in the ionosphere ($\lambda_{\perp i} = \lambda_\perp$ at 100 km altitude) used here are 50 m (black), 200 m (dark blue), 800 m (red) and 3200 m (green).

[17] For the numerical solution of equations (4) and (5) attempted here the boundary condition at the magnetospheric end is as given by *Thompson and Lysak* [1996]. Here the conductivity is set equal to the Alfvén conductivity of the field line in the local approximation. In this case $A_\parallel + 4\pi\Sigma_A(\varphi_o(t) - \varphi)/c = 0$, where $\Sigma_A = c^2/(4\pi E_{\perp 1}/B_{\perp 2})$ and $\varphi_o(t)$ is an applied potential which allows a wave to be launched down the field line from the magnetospheric end. The ratio $E_{\perp 1}/B_{\perp 2}$ is given from the Fourier transform of equations (4) and (5) along B_o and Faraday's law as

$$E_{\perp 1}/B_{\perp 2} = \frac{V_A}{c}\sqrt{\frac{1+k_\perp^2\lambda_e^2}{1+k_\perp^2\left(\rho_i^2+\rho_s^2\right)}}\left(1+k_\perp^2\rho_i^2\right) = E_{\perp 2}/B_{\perp 1}. \quad (8)$$

At the ionospheric end we use the boundary condition derived from current continuity as given by *Lysak* [1991]. This has been modified by *Chaston et al.* [2002b] to allow an arbitrary angle between $k_{\perp 1}$ and the convection electric field, $\mathbf{E}_o = (E_{o1}, E_{o2})$, in the ionosphere. This is given by

$$A_\parallel + \mu_o\Sigma_{Po}\Phi + i\mu_o\Sigma_{P1}\frac{k_{\perp 1}E_{o1}+k_{\perp 2}E_{o2}}{k_\perp^2} - i\mu_o\Sigma_{H1} \cdot\frac{k_{\perp 1}E_{o2}-k_{\perp 2}E_{o1}}{k_\perp^2} = 0, \quad (9)$$

where we have linearized the height integrated Hall and Pedersen conductivities so that $\Sigma_P = \Sigma_{Po} + \Sigma_{P1}$ and $\Sigma_H = \Sigma_{Ho} + \Sigma_{H1}$. Σ_{P1} and Σ_{H1} are given by the solution of a density continuity equation

$$\left(\frac{\partial}{\partial t} + i(v_{o1}k_{\perp 1} + v_{o2}k_{\perp 2})\right)n_1 = Qk_\perp^2 A_\parallel/\mu_o - R\left(2n_o n_1 + n_1^2\right), \quad (10)$$

under the assumption that $\Sigma_{P1} = Pn_1$ and $\Sigma_{H1} = Hn_1$ where $n = n_o + n_1$ is the ionospheric density. Here v_o is the convection velocity given by $\mathbf{E}_o \times \mathbf{B}_o$, with v_{o1} and v_{o2} components of this velocity along the $k_{\perp 1}$ and $k_{\perp 2}$ directions. $Q = \gamma/(e\Delta z)$, where γ is the number of electron pairs produced per electron incident on the ionosphere in the Alfvén wave. Δz is the thickness of current carrying region of the ionosphere. R is the recombination coefficient describing how rapidly ions and electrons recombine after ionization. Greater detail regarding the derivation of this boundary condition can be found in the work of *Lysak* [1986b, 1991]. The important result here is, however, that the complex terms in the ionospheric boundary condition allows for over-reflection from the ionosphere and wave growth.

6. Simulation Results

6.1. Wave Field Model

[18] The solution of equations (4) and (5) subject to the boundary conditions defined above provides us with a three-dimensional (3-D) model (which is periodic in the directions transverse to B_o) for Alfvén waves above the auroral ionosphere. The numerical technique used in solving these equations is the leapfrog method as described by *Thompson and Lysak* [1996]. At each time step the differential equation in the ionospheric boundary condition given by equation (10) is solved using a fourth-order Runge-Kutta technique. For conservation of magnetic flux it is assumed that $k_\perp = 2\pi/\lambda_\perp$ decreases in altitude with the square root of the magnetic field strength from its predefined value in the ionosphere, $k_{\perp i} = 2\pi/\lambda_{\perp i}$. The equilibrium values of Σ_{Po} and Σ_{Ho} are taken as 1 mho. The remaining free parameters in the model follow from *Lysak* [1991] but for this study are not crucial to the result except that they be sufficient for wave growth. This is because we use the model wave fields to study ion motion only once the instability at each $\lambda_{\perp i}$ has been artificially terminated. In this way the ions are accelerated in wave fields whose amplitudes are constant in time at a given altitude for each case considered.

[19] Figure 4a shows the field-aligned Poynting flux of the wave field obtained from the numerical solution to these equations for the case where the perpendicular wavelengths in the ionosphere are $\lambda_{\perp 1i} = \lambda_{\perp 2i} = 800$ m. The black arrows on this plot show the direction of the Poynting flux. The wave is launched from a Gaussian variation in the potential at 10,000 km altitude and travels down the field line toward the ionosphere as an Alfvén wave. The peak in Poynting flux extending from 10,000 km, at t = 0.5 s in the far top left of Figure 4a, down to 100 km, at $t \sim 1.5$ s, corresponds to the traveling wave during this phase of the simulation. The Poynting flux in this wave decreases in altitude due to the partial upward reflection of the wave on the Alfvén speed gradients over this altitude range shown in Figure 3.

[20] When the wave reaches the ionospheric boundary at $t \sim 1.5$ s the incidence of the current carrying electrons in

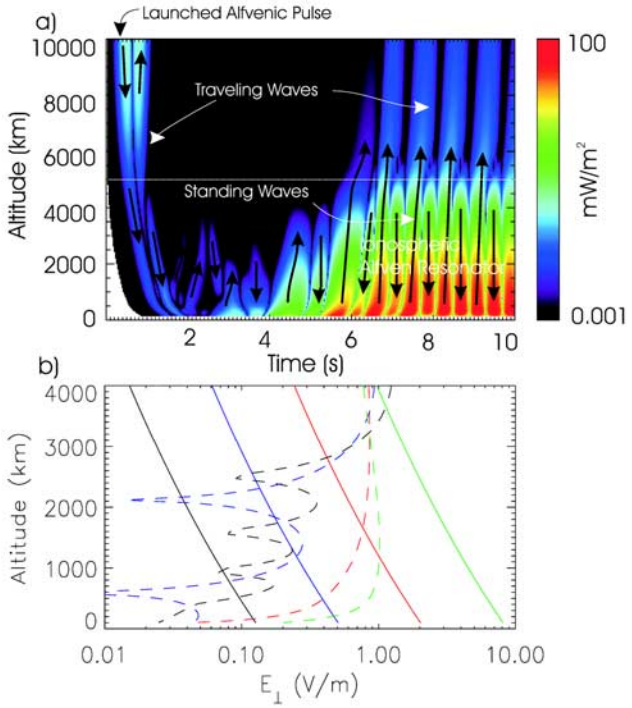

Figure 4. Structure of the ionospheric Alfven resonator. (a) The geomagnetic field aligned wave Poynting flux as a function of altitude and time for $\lambda_{\perp i}$ = 800 m. (b) The amplitude envelopes for $\lambda_{\perp}$ = 50, 200, 800, 3200 m in the black, blue, red, and green dashed lines, respectively. The solid lines show the threshold wave amplitude for stochastic motion from equation (1) for the same $\lambda_{\perp i}$ using the same color scheme.

the wave causes changes in the ionospheric conductivity according to the ionospheric density continuity equation given by equation (10). Strictly speaking, it is the electrons resonantly accelerated by the wave rather than those carrying the wave current which will be the most effective in ionizing the ionospheric plasma. However, for simplicity, the field-aligned wave current has in this case been used. This has the effect of slowing the growth rate and altering the phase relationship between the conductivity variations in the ionosphere and the wave field. After t = ~1.5 s the Poynting flux oscillates between upward and downward directions as the wave is trapped between the ionosphere and the Alfvén speed gradients above it. This is the ionospheric Alfvén resonator [*Polyakov and Rapoport*, 1981; *Traktengertz and Feldstein*, 1984; *Lysak*, 1991; *Lysak and Song*, 2002]. From the boundary condition given by equation (9), the ionospheric conductivity variation, in the presence of a convection electric field, may lead to an overreflection of the wave from the ionosphere. This provides growth in wave amplitude or Poynting flux within the resonator in time as shown on the right side in Figure 4a. This is the ionospheric feedback instability as described by *Lysak* [1991] and *Streltsov and Lotko* [2003].

[21] The frequency of the unstable resonating fluctuations driven by this instability is set by the wave phase speed, dimensions of the resonant cavity, the convection speed in the ionosphere (v_o), and the angle between $\mathbf{k}_{\perp 1}$ and $\mathbf{v}_o$. For simplicity and since we are modeling observations near midnight, we have chosen $\mathbf{k}_{\perp 1}$ to lie along $\mathbf{v}_o$. In this case, convection drives the wave with frequency $\omega = k_{\perp 1} v_o$. For the example wave field model shown in Figure 4 we have used a convection electric field of 25 mV/m. This provides a wave frequency in the resonator for $k_{\perp 1i} = 2\pi/800$ m of 0.6 Hz In a standing wave this frequency will be one half of the frequency of the oscillations in S_z.

[22] In the test ion calculations which follow, the $\lambda_{\perp i}$ of the wave field considered are 3200 m, 800 m, 200 m, and 50 m. These values cover the range of observed scales shown in Figure 2c. The convection electric field for each is taken as Eo = 100.00, 25.00, 6.25, and 3.125 mV/m, respectively, which provide a wave frequency in the resonator of ~0.6 Hz in each case. The constant frequency has been chosen to eliminate variations due to wave frequency in the ion motion in the wave field for differing $k_{\perp}$, and for consistency with the result from the observations section that showed $\omega < \Omega_{O+}$. These convection fields are within the range of convection fields identified by *Vondrak* [1981] in auroral arcs. The wave in each case is allowed to grow until it reaches an amplitude of 1 V/m at some altitude (usually from 4000 to 8000 km). On reaching this condition the instability is turned off by fixing the magnitude of the conductivity oscillations. After this time the wave amplitude remains invariant through the reminder of the simulation. It is the wave fields from this phase of the simulation that are used to study ion acceleration. In Figure 4a this occurs on the far right at t = 7 s.

[23] The wave envelopes generated from the feedback instability for each scale considered are given by the dashed lines in Figure 4b. For the waves with $\lambda_{\perp i}$ = 3200 m (green) and 800 m (red), the fundamental of the resonator is excited with a node at the ionosphere and an anti-node at the top end of the resonator at ~5000 km. For the $\lambda_{\perp i}$ = 200 m (blue) and 50 m (black) cases the second and third harmonics are excited, respectively. For the smaller perpendicular wave scales used here the parallel wavelength of the oscillations may become comparable to the thickness of the ionosphere. In this case the parallel resistivity of the ionosphere may lead to significant wave damping not incorporated in the model described in section 5 [*Borovsky*, 1993; *Lysak and Song*, 2002; *Streltsov and Lotko*, 2003]. For a horizontally uniform ionospheric conductivity, *Lessard and Knudsen* [2001] find that reflection from the ionosphere at $\lambda_{\perp i} < 1$ km is negligible. Consequently, inclusion of the parallel resistivity in our simulation results can be expected to show that the ionospheric Alfvén resonator will be strongly damped at the 200 m and 50 m scales used. We reserve the inclusion of this effect for a later study describing ion acceleration in a spectrum of waves driven by the ionospheric Alfvén resonator. For the results of this study, however, where $\lambda_{\perp}$ is preset and based on the wave scales observed, the actual mechanism generating the wave fields is not of great importance in determining if these waves can accelerate ions. By using the feedback instability of the ionospheric Alfvén resonator, we define the amplitude variation of the wave with altitude. It is likely at the smaller scales observed that the waves are in fact generated by a different process [*Seyler*, 1990; *Seyler et al.*, 1998; *Passot and Sulem*, 2003; *Wu and Seyler*, 2003]. These waves are, however, still Alfvénic and, as demonstrated by

Stasiewicz et al. [2000b], obey the dispersion relation given by equation (7) as modeled here.

6.2. Ion Acceleration

[24] The equation of motion of the ions is given by

$$m\frac{dv}{dt} = q\mathbf{E} + qv \times \mathbf{B}t + m\left(0, 0, GM_e/r^2\right), \qquad (11)$$

where m is the ion mass, $B_t = B_o + B$ is the total magnetic field, E and B are the wave electric field and magnetic fields, $G = 6.6726 \times 10^{-11}$ m^3 s^{-2} kg^{-1} is the gravitational constant, $Me = 5.98 \times 10^{24}$ kg is the Earth's mass, and r is the radial distance of the ion from the Earth's center. This equation is solved using a standard fourth-order Runge-Kutta technique. Using this approach, we find that by taking 100 or more time steps per gyroperiod simulation runs provide final energies differing by 5% or less. The accuracy of this approach has also been tested by comparing the numerical ion trajectory with the analytical result in the absence of a wave field. In the simulation results presented in this report, 200 time steps per gyroperiod are used.

[25] The forces acting on the ions and contained in equation (11) include the Lorentz force due to the electromagnetic fields and gravitation. Contributions to the Lorentz force can be independently considered as those due to the geomagnetic and wave fields. The geomagnetic field provides the gyromotion of the ions and the mirror force due to the magnetic moment of the rotating ion in the divergent geomagnetic field. Above the auroral oval, an approximate inverse cubic dependence of the geomagnetic field with geocentric distance (r^{-3}) provides a mirror force given by 3/2 m $v_\perp^2$/r acting outward. This means that at an altitude of 200 km, O^+ and H^+ ions require transverse energies greater than ~3.4 eV and ~0.2 eV, respectively, to escape the Earth's gravitational field. Ions with energies larger than these values at this altitude will contribute to ion outflow from the auroral ionosphere.

[26] The perpendicular electric wave field, $E_\perp$, accelerates the ions in the transverse direction and is the most important component of the wave field for modifying the gyromotion. The parallel electric wave field $E_\parallel$ is ineffective at imparting significant energies to the ions because the parallel wave phase speed is much larger than the parallel ion velocity. This field provides minor oscillations in the ion energy parallel to B_o at the wave frequency. The amplitude of the magnetic wave field is several orders of magnitude smaller than the geomagnetic field over the altitude range considered and has little effect on the ion motion. Ambipolar fields associated with the differential acceleration of ions and electrons are ignored. These fields can be expected lead to the outward acceleration of electrons with the ions to maintain charge neutrality. Given that the mass ratio of the ions to the electrons is at least the proton/electron mass ratio, the drag on the outward ion motion due to the electrons can be expected to have little impact on the final ion energies obtained in this study.

[27] Figure 5 shows the results from tracing an O^+ ion with an initial perpendicular energy of 1 eV in the model wave field with $k_{\perp 1} = k_{\perp 2}$ and $k_{\perp i} = 2\pi/800$ m. A time span slightly greater than a wave period is shown. The contours represent a snapshot of the field-aligned current in the wave at t = 0. The red traces show the ion trajectory in the plane perpendicular to B_o. Figures 5a and 5b show the result when the ion is injected into the model wave field at an altitude of 200 km altitude. In this case the wave begins with a phase such that $E_{\perp 1}$ is at a maximum. Over a time span equivalent to a quarter wave period, Figure 5a shows that the gyrodiameter of the ion grows to nearly reach $\lambda_\perp$. Over the next quarter cycle the reversal in the sense of the wave field results in the ion losing this energy before regaining it in the next quarter cycle and so on to provide oscillations in ion energy. This is the motion of an ion trapped in the wave potential of a large-amplitude coherent wave as described by *Karney and Bers* [1977], *Karney* [1978], *Lysak et al.* [1980], and *Lysak* [1986a]. The ratio of ω/Ω_{O+} at this altitude is 0.011 and $\Omega_{O+}/k_\perp$ is 36,823 ms^{-1}. From Figure 4b the wave amplitude at this altitude is 200 mVm^{-1}, which provides an $E_\perp/B_o$ ratio of 3900 ms^{-1}. Clearly, $E_\perp/B_o \ll \Omega_{O+}/k_\perp$, and so from the threshold conditions for stochastic behavior given by *Chen et al.* [2001] and *Karney* [1978] the ion motion is expected to be coherent, as indeed it is.

[28] Figures 5c and 5d show the same quantities for an oxygen ion injected into the wave model at an altitude of 4000 km. The ion motion is this case can be seen to be randomized, and the ion on average gains energy. The ratio ω/Ω_{O+} at this altitude is 0.042 and $\Omega_{O+}/k_\perp$ is 4768 ms^{-1}. From Figure 4b the wave amplitude at this altitude is 1 Vm^{-1}, which provides an $E_\perp/B_o$ ratio of 72,000 ms^{-1}. Clearly, $E_\perp/B_o \gg \Omega_{O+}/k_\perp$, and so from the threshold conditions given by *Chen et al.* [2001] and *Karney* [1978], the ion motion is expected to be stochastic as indeed it is.

6.3. Ion Outflow

[29] Clearly, both the coherent and stochastic ion acceleration mechanisms can supply energy to the ions sufficient to overcome gravity. To now examine the ability of Alfvén waves to provide ion outflow above the aurora, we trace the ion motion over many wave periods from an initial altitude and transverse energy of 200 km and 1 eV, respectively. The results from tracing hydrogen (H^+) (dashed lines) and oxygen (O^+) ions (solid lines) for a number of different perpendicular wavelengths (green→$\lambda_\perp i$ = 3200 m, red→800 m, blue→200 m, black→50 m) with $\lambda_{\perp 1} = \lambda_{\perp 2}(k_{\perp 1} = k_{\perp 2})$ is shown in Figure 6. Distinguishing the two kinds of transverse ion motion from these curves is essential to understanding the process by which the ions are accelerated as they stream outward. As demonstrated in section 6.2, this can be achieved from an examination of the ion orbit. However, when tracing the motion of outflowing ions from the ionosphere to altitudes of 1 Re, it is not practical to retain position and velocity information at subgyroperiod resolution. These different forms of ion motion can however be distinguished by exploiting the fact that in the coherent or trapped motion case the maximum energy of the ions is related to the perpendicular scale of the wave [*Lysak et al.*, 1980]. A simple way to identify the transition from coherent/trapped ion motion to stochastic motion is then to plot the effective ion gyroradii normalized by the perpendicular wavelength of the wave. The transition from coherent to stochastic motion can then be readily identified by sudden jumps followed by unstructured variations in this ratio. This technique has been used to

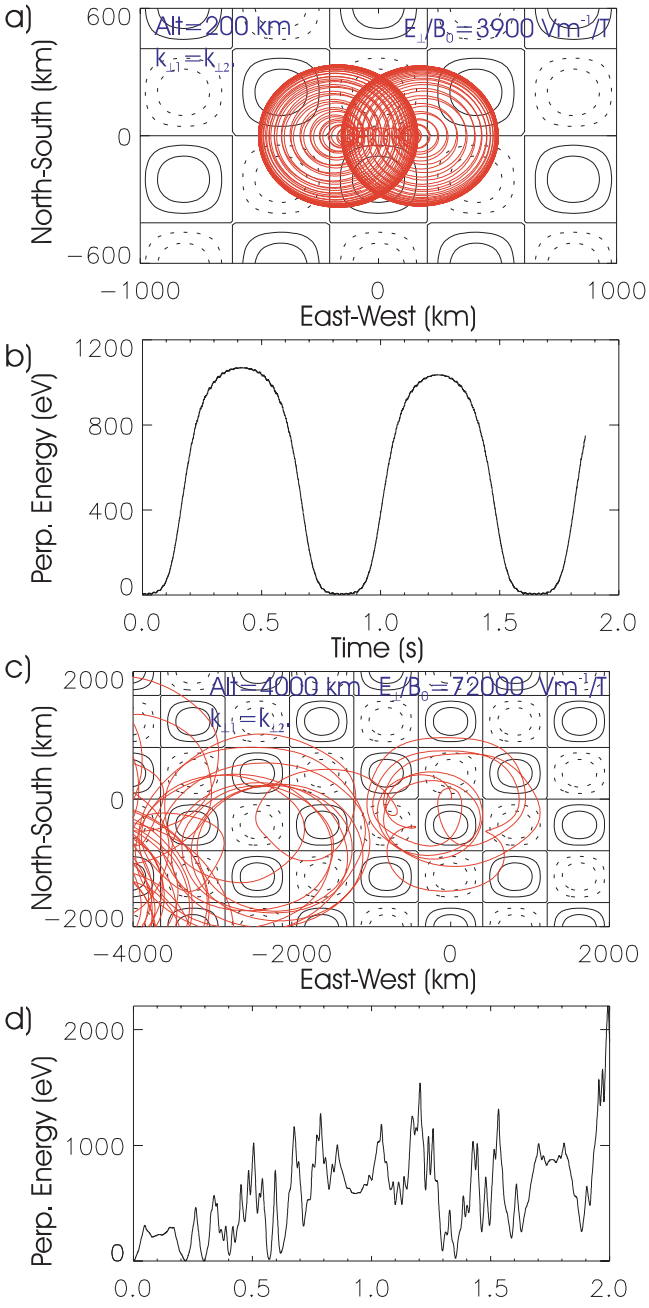

Figure 5. O^+ trajectories over slightly more than a wave period for $k_{\perp1} = k_{\perp2}$ where $k_{\perp1i} = 2\pi/800$ m. (a) The trajectory of an O^+ ion at an altitude of 200 km. The contours represent the field-aligned current carried by the waves with dashed contours being upward current and solid contours downward current. (b) The energy of the O^+ ion along the trajectory shown in Figure 5a. (c) The trajectory of an O^+ ion at an altitude of 4000 km with the contours as in Figure 5a. (d) The energy of the O^+ ion along the trajectory shown in Figure 5c.

label those periods where the ion motion is consistent with coherent/trapped ion motion in Figures 6c–6f.

6.3.1. Coherent/Trapped Ion Motion and Finite Gyroradius Effects

[30] At low altitudes, where $E_\perp/B_o$ is smallest, Figure 6 shows that the ion motion is predominately coherent. From Figure 6a it can be seen that the largest perpendicular wavelength ($\lambda_{\perp i}$ = 3200 m, green lines) provides the most rapid outflow of ions. H^+ ions are accelerated from 200 km up to FAST apogee (4000 km) in 2 or more seconds with O^+ ions reaching this altitude in 16 or more seconds. The rate of ascent decreases with decreasing perpendicular scale until at $\lambda_{\perp i}$ = 50 m (black lines) O^+ ions fail to be elevated at all over the time scale plotted here. Figure 6b shows the field-aligned energy of these ions as they stream outward. The

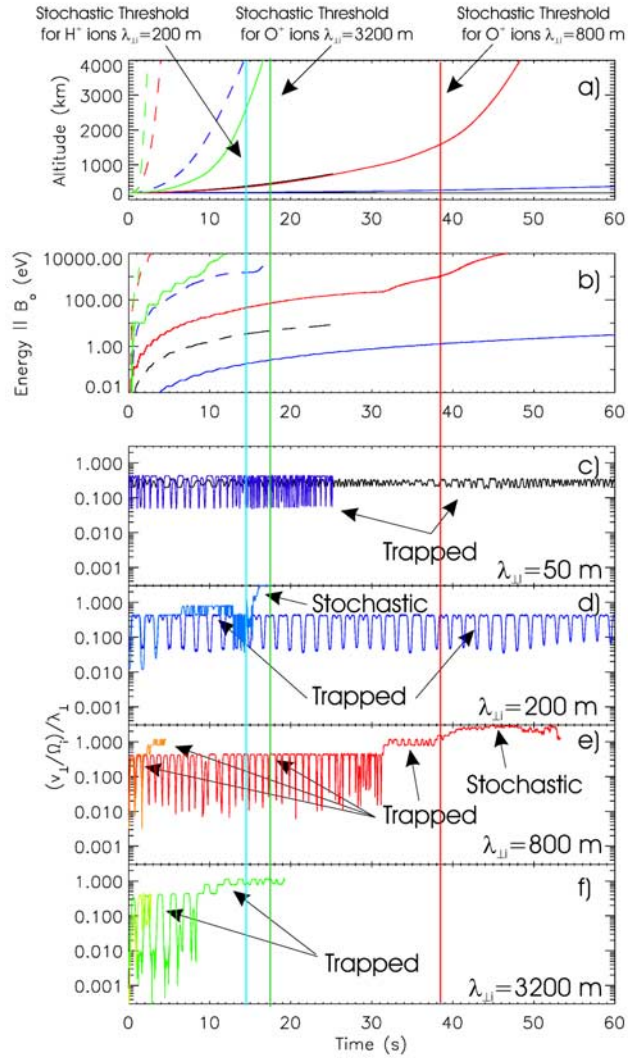

Figure 6. Wave number dependency of ion acceleration. The vertical lines show the time at which the ions reach an altitude where the amplitude equals the threshold for stochastic motion given by equation (1) with $\alpha = 1$. (a) The altitude reached by ions as a function of time. The dashed lines here are for H^+ ions while the solid lines are for O^+. Green lines are for perpendicular wavelengths in the ionosphere of $\lambda_{\perp1i} = \lambda_{\perp2i}$ = 3200 m, red is $\lambda_{\perp1i} = \lambda_{\perp2i}$ = 800 m, blue is $\lambda_{\perp1i} = \lambda_{\perp2i}$ = 200 m, and black is $\lambda_{\perp1i} = \lambda_{\perp2i}$ = 50 m. (b) The field-aligned energy of the accelerated ions. (c)–(f) The ion gyroradii normalized by the perpendicular wavelength using the same color code as Figures 2a and 2b. Light lines are for H^+ ions, while the darker lines are for O^+.

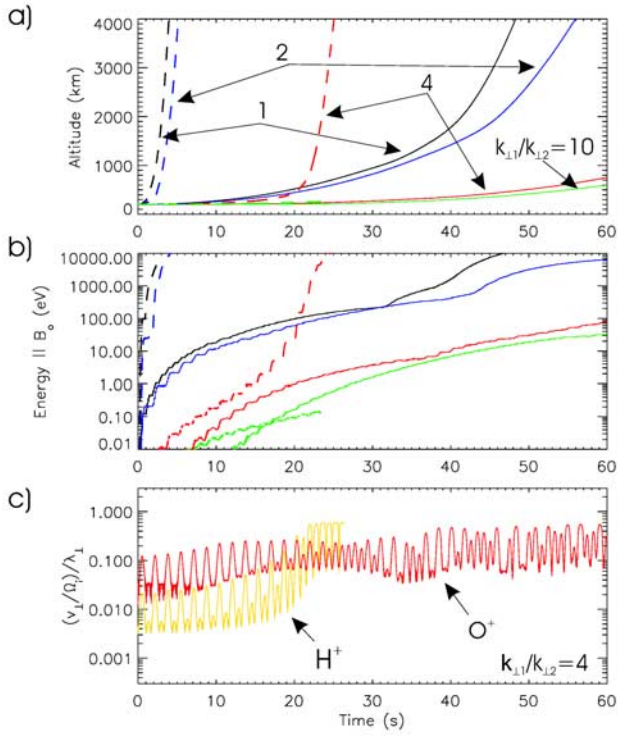

Figure 7. The $k_{\perp 1}/k_{\perp 2}$ dependency of ion acceleration for $\lambda_{\perp 1i}$ = 800 m. (a) The altitude reached by ions as a function of time. The dashed lines here are for H^+ ions, while the solid lines are for O^+ ions. Green lines are for the perpendicular wave number ratio of $k_{\perp 1}/k_{\perp 2}$ = 10, while red is for $k_{\perp 1}/k_{\perp 2}$ = 4, blue is for $k_{\perp 1}/k_2$ = 2, and black is for $k_{\perp 1}/k_{\perp 2}$ = 1. (b) The field-aligned energy of the accelerated ions. (c) The ion gyroradii normalized by the perpendicular wavelength for $k_1/k_{\perp 2}$ = 4, with the orange line the result for H^+ ions and the red line the result for O^+ ions.

waves with larger $\lambda_\perp$ provide larger ion energies. For the field amplitudes obtained from the simulation, we find energies extending up to 10 keV over the FAST altitude range. Hydrogen ions gain more energy than oxygen ions. Perpendicular energies, while not shown here, are generally larger than the field-aligned energy particularly at the lowest altitudes considered.

[31] The dependency of the energies obtained on the perpendicular scale of the wave can be understood by considering the ratio of the ion gyroradii to $\lambda_\perp$ shown in Figures 6c–6f. For most of the time range plotted the upper limit of the oscillations in this quantity occurs when the gyroradii is roughly half the perpendicular wavelength of the wave. This is similar to the upper limit derived by *Lysak et al.* [1980], as discussed in section 2. In a uniform background magnetic field, with large wave amplitudes and $\lambda_{\perp 1} = \lambda_{\perp 2}$, this provides an average energy gain over the first wave cycle but not afterward. Above the auroral oval, however, the mirror force associated with the divergent geomagnetic field, if sufficient to overcome gravity, accelerates these oscillating ions upward. Given that magnetic flux is conserved, $\lambda_\perp$ increases with altitude, and so the upward motion of the ions allows them to continue to gain in average energy on each wave cycle yet still maintain gyrodiameters less than or equal to the approximate upper limit of $\lambda_\perp$.

[32] The mass dependency of the acceleration is also a result of the finite perpendicular wave scale. For the same gyroradius, H^+ ions have 16 times the energy of O^+ ions, so from the results shown in Figure 6, where the gyroradii limit is reached, the H^+ ions are more energetic. This also explains why at $\lambda_{\perp 1i}$ = 50 (black lines in Figure 4a) H^+ ions can gain altitude while O^+ ions do not. This is because the transverse energy corresponding to a gyroradius of 25 m for an oxygen ion at 200 km altitude provides a mirror force barely sufficient to overcome gravity. H^+ ions, however, can gain energy, in waves of this scale and smaller, sufficient to escape the Earth's gravitation and contribute to auroral ion outflow.

[33] While larger scales can provide greater energies, spacecraft observations suggest that the effectiveness of scales larger than ~1 km for accelerating the ions may be limited. Larger scales require larger wave amplitudes to provide sufficient gradients in $E_\perp$(particularly in the case of H^+) to yield acceleration up to the gyroradii limit. Furthermore, the ratio of $\lambda_{\perp 1}/\lambda_{\perp 2}$ must be sufficiently close to 1 for any gyroaveraged acceleration to occur. Figure 7 shows the effect of increasing $\lambda_{\perp 2i}$ relative to $\lambda_{\perp 1i}$, where $\lambda_{\perp 1i}$ is held fixed at 800 m. It can be seen from this plot that when $\lambda_{\perp 2}$ is an order of magnitude larger than $\lambda_{\perp 1}$, then acceleration (for the wave amplitudes considered here) effectively ceases and the ions E × B drift in the wave field. By generalizing the treatment of *Chen* [1984, pp. 36] to include large $k_\perp \rho_i$, it can be shown that the speed of this drift is given by $\overline{v}_{\perp 2} = (E_{\perp 1}(x)/B_o)J_o(k_\perp \rho_i)$, where J_o is the zeroth order Bessel function and the overline refers to an average over a gyroperiod. In this limit the ions gain no energy. For intermediate values of $\lambda_{\perp 1}/\lambda_{\perp 2}$ the upper energy limit is still set by the gyrodiameter reaching the smaller of $\lambda_{\perp 1}$ or $\lambda_{\perp 2}$. However, it can be seen from Figure 7c, for the case where $\lambda_{\perp 2}/\lambda_{\perp 1}$ = 4, that the time taken to reach this condition is much longer. Given that Freja and FAST observations suggest that these waves become increasing laminar beyond perpendicular scales of the order of 1 km [*Volwerk et al.*, 1996; *Stasiewicz et al.*, 2000b] indicates that the most important scales responsible for ion outflow in this process most likely lie below 1 km. Furthermore, observations show ion energies from 100 to 1000 eV. These energies correspond to energization via the coherent process for waves with $\lambda_\perp$ < 650 m for H^+ and 2600 m for O^+. These scales are in the middle of the observed range of scales identified from observations in section 3.

6.3.2. Stochastic Particle Motion

[34] At higher altitudes, $E_\perp/B_o$ may be large enough for the particle gyromotion to be disrupted to allow the ions to gain energy in excess of that determined by $\lambda_\perp$. The first signs of this disruption can be seen in Figures 6c–6f where at altitudes above 1000 km the ions perform step-like jumps in $\rho_i/\lambda_\perp$ as the ion moves from one trapped orbit to another. The magnitude of each step is roughly equivalent to the energy required for a jump in gyroradii of half $\lambda_\perp$. The threshold wave amplitudes required for the stochastic motion of O^+ ions (from equation (1)), as a function of altitude, are presented by the solid color lines in Figure 4b. (The threshold amplitudes for H^+ are 16 times larger than shown here.) The dashed lines in this figure show the wave amplitude envelopes of the wave models used as discussed previously in section 6.1. Where

these dashed lines intersect the solid lines of the same color or extend to the right of the solid line of the same color, then according to equation (1), stochastic ion motion is possible at that scale. This indicates that the predicted threshold amplitude for stochastic motion is exceeded for O^+ at altitudes as low as 500 km for $\lambda_\perp = 50$ m. H^+ ion motion may become stochastic at altitudes above 3000 km for the same scale. In general these curves show that the altitude at which stochastic motion is predicted to occur increases with increasing perpendicular scale of the wave.

[35] The accuracy of the predicted threshold from equation (1) can be tested numerically. The vertical colored lines in Figure 6 show the time at which an ion reaches the altitude where the wave amplitude exceeds the stochastic threshold given by equation (1). For the 1-min time span of the simulation this altitude is attained only by H^+ ions in the $\lambda_{\perp i} = 200$ m wave field shown in Figure 6d and O^+ ions in the $\lambda_{\perp i} = 800$ and 3200 m wave fields shown in Figures 6e and 6f. In each of these cases the particle motion becomes stochastic shortly after this threshold is exceeded. This is in agreement with equation (1).

[36] The energy gain in the stochastic phase can be much larger than possible from coherent ion motion, since it is not limited by the perpendicular scale of the wave. Even on the log plot for parallel ion energy shown in Figure 6b, the onset of stochastic motion can be seen to lead to an increased rate of energy gain. In the cases studied here, we find energies extending to above 10 keV. This represents an upper limit to energies obtained by this process. This is not because we have reached the upper limit of the stochastic domain but because we have used amplitudes close the maximum amplitudes observed for these waves and have assumed that the wave field extends continuously along and across the geomagnetic field. In reality the distribution of the observed wave fields while extended along B_o may be localized in the transverse direction. Consequently, the ions may wander across flux tubes where waves are not found rather than being continuous immersed and heated in the wave field as modeled here. Obviously, this can be expected to lead to lower final energies.

[37] Therefore for an ion accelerated from 200 km, the acceleration initially proceeds via the coherent process until the ions have reached altitudes where $E_\perp/B_o > \Omega_i/k_\perp$ and the ion motion may become stochastic. In the case where multiple waves are present and wave frequencies are higher than used here the stochastic threshold may be significantly less than obtained in this case [*Karney*, 1978; *Lysak et al.*, 1980; *Chen et al.*, 2001]. However, the single wave, low-frequency results from this study indicate that ion acceleration in dispersive Alfvén waves above the auroral oval is likely. Particles may be accelerated by this process from energies of the order of an eV into the keV range. This acceleration may occur in a coherent or stochastic manner. Coherent acceleration is expected to be most important at lower altitudes with stochastic acceleration becoming important with increasing altitude above 1000 km due to the weakening geomagnetic field and strengthening Alfvén wave electric fields.

7. Conclusions

[38] Observations from the FAST satellite suggest a relationship between intense fluxes of transversely energized ions and Alfvén waves. It has been demonstrated, by tracing the motion of ions in a realistic model for Alfvén waves above the aurora, that dispersive Alfvén waves, with frequency a small fraction of the local ion gyrofrequency, may provide rapid ion acceleration and outflow from the auroral oval. This has been shown from simulations to occur in waves within the range of observed amplitudes when the waves' perpendicular wavelength approaches the ion gyroradii. Observations using interferometric techniques show that the observed perpendicular scales (or wavelengths) cover a range extending from larger than the electron inertial length (tens of kilometers) down to energetic hydrogen gyroradii (tens of meters). Consequently, it seems likely that ions in the aurora will be accelerated by Alfven waves. These ions may be accelerated by two processes.

[39] 1. Coherent ion acceleration: Simulations show that ions moving coherently in the wave field may be accelerated transverse to B_0 up to energies where the gyroradii is approximately half the perpendicular wavelength. The ion energy in this case is oscillatory with gains in average energy made through the upward acceleration of the ion under the influence of the mirror force and increasing $\lambda_\perp$ with altitude. The rate of ion acceleration in the wave is highly dependent on the ratio of wave numbers ($k_{\perp 1}$, $k_{\perp 2}$) transverse to B_o. There is no acceleration by this means in the plane wave case (i.e., $k_{\perp 1} = 0$ or $k_{\perp 2} = 0$). Observations show energies for the ion species present up to 1 keV. If this process is operating, then at the altitude of observation shown in Figure 1, the acceleration occurs in waves with $\lambda_\perp$ less than 650 m for H^+ ions and less than 2600 m for O^+ ions. Interferometry, using FAST satellite observations, show that these $\lambda_\perp$ are in the middle of the range of perpendicular scales observed.

[40] 2. Stochastic ion acceleration: Alternatively, ion acceleration may occur through a process where the ion trajectory through the wave field becomes stochastic. It has been shown that the electric field amplitudes required for stochastic ion motion above the auroral oval are within the range of observations. Stochastic motion is more likely for O^+ than H^+ and more likely at higher altitudes where B_o is weaker and $E_\perp$ larger. This is found to be roughly consistent with the theory of *Chen et al.* [2001] where the ion motion may become stochastic when $E_\perp/B_o > \Omega_i/k_\perp$. For the large-amplitude cases simulated here, this process may provide ion energies exceeding 10 keV and account for higher O^+ than H^+ energies.

[41] The simulation results suggest that ion acceleration in the Alfven wave field from the topside ionosphere occurs through a combination of the above two mechanisms. For a single monochromatic wave with amplitude within the range of observations, the ion motion at low altitudes is coherent, allowing acceleration up to the limit set by the waves perpendicular scale. As the ion moves upward the weakening geomagnetic field and the increasing wave amplitude allows the ion motion to become stochastic so that higher energies may be reached. This two-step acceleration process moves ions from 200 km to 1 Re in altitude over times ranging from seconds to less than 1 min and may provide ion energies exceeding 10 keV. It should be remembered, however, that in this study we have considered ion acceleration in a continuous wave field extending infinitely in the transverse direction and with amplitudes at the upper

end of those observed. Because of this, these results represent the upper limit for the final energies reached and a lower limit for the timescales required to reach 1 Re in altitude from the ionosphere. Exactly how the results differ from those where the ions are accelerated over a spectrum of perpendicular wave numbers and frequencies remains a topic for future study.

[42] Finally, we have shown how the required wave fields may be generated through the ionospheric feedback instability. In reality this instability may be strongly damped at the smallest scales considered. However, it is not essential for the waves to be generated in this way for the ion acceleration process to occur in the manner described here. Indeed any wave with perpendicular scaling of the order of the ion gyroradii of sufficient amplitude and $\omega < \Omega_p$ may provide acceleration via the same means. The feedback instability is, however, particularly effective as a energy supply for ion outflow above the ionosphere as it can sustain large amplitudes at low altitudes in the source regions for outflowing ions.

[43] **Acknowledgments.** This research was supported by NASA grants NAG5-3596, NAG5-12954, and NAG5-12784. Chris Chaston is indebted to Chu Ming Chung and the physics department at the Chinese University of Hong Kong where some of this research was completed.

[44] Lou-Chuang Lee thanks Robert L. Lysak and another reviewer for their assistance in evaluating this paper.

References

Andre, M., and A. Yau (1997), Theories and observations of ion acceleration and outflow in the high latitude magnetosphere, *Space Sci. Rev.*, *80*, 27.

Borovsky, J. E. (1984), The production of ion conics by oblique double layers, *J. Geophys. Res.*, *89*, 2251.

Borovsky, J. E. (1993), Auroral arc thicknesses as predicted by various theories, *J. Geophys. Res.*, *98*, 6101.

Chaston, C. C., J. W. B. Bonnell, J. P. McFadden, R. E. Ergun, and C. W. Carlson (2001a), Electromagnetic ion cyclotron waves at proton cyclotron harmonics, *J. Geophys. Res*, *107*(A11), 1351, doi:10.1029/2001JA900141.

Chaston, C. C., J. W. Bonnell, C. W. Carlson, M. Berthomier, L. M. Peticolas, I. Roth, J. P. McFadden, and R. J. Strangeway (2001b), Electron acceleration in the ionospheric Alfvén resonator, *J. Geophys. Res.*, *107*(A11), 1413, doi:10.1029/2002JA009272.

Chaston, C. C., J. W. Bonnell, C. W. Carlson, R. E. Ergun, J. P. McFadden, and R. J. Strangeway (2003a), Properties of small scale Alfvén waves and accelerated electrons from FAST, *J. Geophys. Res.*, *108*(A4), 8003, doi:10.1029/2002JA009420.

Chaston, C. C., L. M. Peticolas, J. W. Bonnell, C. W. Carlson, R. E. Ergun, and J. P. McFadden (2003b), Width and brightness of auroral arcs driven by inertial Alfvén waves, *J. Geophys. Res.*, *108*(A2), 1091, doi:10.1029/2001JA007537.

Chaston, C. C., J. Bonnell, C. W. Carlson, J. P. McFadden, R. E. Ergun, and R. J. Strangeway (2003c), Kinetic effects in the acceleration of electrons by small scale Alfvén waves: A FAST case study, *Geophys. Res. Lett.*, *30*(6), 1289, doi:10.1029/2002GL015777.

Chen, F. F. (1984), *Introduction to Plasma Physics and Controlled Fusion*, vol. 1, *Plasma Physics*, p. 36, Plenum, New York.

Chen, L., Z. Lin, and R. White (2001), On resonant heating below the cyclotron frequency, *Phys. Plasmas*, *8*, 4713.

Cole, K. (1976), Effects of crossed magnetic and (spatially dependent) electric fields on charged particle motion, *Planet. Space Sci.*, *24*, 515.

Collin, H. L., and R. G. Johnson (1985), Some mass dependent features of energetic ion conics over the auroral regions, *J. Geophys. Res.*, *90*, 9911.

Genot, V., P. Louarn, and F. Mottez (2004), Alfvén wave interaction with inhomogeneous plasmas: Acceleration and cascade towards small scales, *Ann. Geophys.*, in press.

Greenspan, M. E. (1984), Effects of oblique double layers on upgoing pitch angle and gyrophase, *J. Geophys. Res.*, *89*, 2842.

Hultqvist, B., , M. Oieroset, G. Paschmann, and R. Trueman (Eds.) (1999), Magnetospheric Plasma Sources and Losses, Space Sci. Ser. of ISSI, Kluwer Acad., Norwell, Mass.

Johnson, J. R., and C. Z. Cheng (2001), Stochastic ion heating at the magnetopause due to kinetic Alfvén waves, *Geophys. Res. Lett*, *28*, 4421.

Karney, C. F. (1978), Stochastic heating by a lower hybrid wave, *Phys. Fluids*, *21*, 1584.

Karney, C. F., and A. Bers (1977), Stochastic ion heating by a perpendicularly propagating electrostatic wave, *Phys. Rev. Lett.*, *39*, 550.

Knudsen, D. J., and J.-E. Wahlund (1998), Core ion flux bursts within solitary kinetic Alfvén waves, *J. Geophys. Res.*, *103*, 4157.

Knudsen, D. J., B. A. Whalen, T. Abe, and A. Yau (1994), Temporal evolution and spatial dispersion of ion conics: Evidence for a polar cusp heating wall, in *Solar System Plasmas in Space and Time*, *Geophys. Monogr. Ser.*, vol. 84, edited by J. L. Burch and J. H. Waite Jr., p. 163, AGU, Washington, D. C.

Lessard, M. R., and D. J. Knudsen (2001), Ionospheric reflection of small-scale Alfvén waves, *Geophys. Res. Lett.*, *28*, 3573.

Li, X., and M. Temerin (1993), Ponderomotive effects on ion acceleration in the auroral zone, *Geophys. Res. Lett.*, *20*, 13.

Lund, E. J., et al. (2000), Transverse ion acceleration mechanisms in the aurora at solar minimum: Occurence distributions, *J. Atmos. Terr. Phys.*, *62*, 467.

Lysak, R. L. (1986a), Ion acceleration by wave-particle interaction, in *Ion Acceleration in the Magnetosphere and Ionosphere*, *Geophys. Monogr. Ser.*, vol. 38, edited by T. S. Chang, p. 261, AGU, Washington, D. C.

Lysak, R. L. (1986b), Coupling of the dynamic ionosphere to auroral flux tubes, *J. Geophys. Res.*, *91*, 7047.

Lysak, R. L. (1991), Feedback instability of the ionospheric resonant cavity, *J. Geophys. Res.*, *96*, 1553.

Lysak, R. L., and C. W. Carlson (1981), Effect of microscopic turbulence on magnetosphere-ionosphere coupling, *Geophys. Res. Lett.*, *8*, 269.

Lysak, R. L., and X. Lotko (1996), On the kinetic dispersion relation for shear Alfvén waves, *J. Geophys. Res.*, *101*, 5085.

Lysak, R. L., and Y. Song (2002), Energetics of the ionospheric feedback interaction, *J. Geophys. Res.*, *107*(A8), 1160, doi:10.1029/2002JA009406.

Lysak, R. L., M. K. Hudson, and M. Temerin (1980), Ion heating by electrostatic ion cyclotron turbulence, *J. Geophys. Res.*, *85*, 678.

Norqvist, P., M. Andre, L. Eliasson, A. I. Eriksson, L. Bloomberg, H. Luhr, and J. H. Clemmons (1996), Ion cyclotron heating in the dayside magnetosphere, *J. Geophys. Res.*, *101*, 13,179.

Papadopoulos, K., J. D. Gaffey Jr., and P. J. Palmadesso (1980), Stochastic acceleration of large M/Q ions by hydrogen cyclotron waves in the magnetosphere, *Geophys. Res. Lett.*, *11*, 1014.

Passot, T., and P. L. Sulem (2003), Filamentation instability of long Alfvén waves in warm collisionless plasmas, *Phys. Plasmas*, *10*, 3914.

Penano, J., and G. Ganguli (2000), Generation of ELF electromagnetic waves in the ionosphere by localized transverse dc electric field: Sub-cyclotron frequency range, *J. Geophys. Res.*, *105*, 7441.

Polyakov, S., and V. O. Rapoport (1981), The ionospheric Alfven resonator, *Geomagn. Aeron.*, *21*, 816.

Ram, A. K., A. Bers, and D. Benisti (1998), Ionospheric ion acceleration by multiple electrostatic waves, *J. Geophys. Res.*, *103*, 9431.

Reitzel, K. J., and G. J. Morales (1996), Perpendicular ion acceleration in field-aligned density striations, *J. Geophys. Res.*, *101*, 27,177.

Seyler, C. E. (1990), A mathematical model of the structure and evolution of small-scale discrete auroral arcs, *J. Geophys. Res.*, *95*, 17,199.

Seyler, C. E., A. E. Clark, J. Bonnell, and J.-E. Wahlund (1998), Electrostatic broadband ELF wave emission by Alfvén wave breaking, *J. Geophys. Res.*, *103*, 7027.

Stasiewicz, K., et al. (2000a), Stochastic ion heating by orbit chaotization on electrostatic waves and non-linear structures, *Phys. Scr. T*, *84*, 60.

Stasiewicz, K., et al. (2000b), Small scale Alfvénic structure in the aurora, *Space Sci. Rev.*, *92*, 423.

Stasiewicz, K., Y. Khotyaintsev, M. Berthomier, and J. E. Wahlund (2000c), Identification of widespread turbulence of dispersive Alfvén waves, *Geophys. Res., Lett.*, *27*, 173.

Streltsov, A., and W. Lotko (2003), Small-scale electric fields in downward auroral current channels, *J. Geophys. Res.*, *108*(A7), 1289, doi:10.1029/2002JA009806.

Thompson, B. J., and R. L. Lysak (1996), Electron acceleration by inertial Alfvén waves, *J. Geophys. Res.*, *101*, 5359.

Traktengertz, V. Y., and A. Y. Feldstein (1984), Quiet auroral arcs: Ionospheric effect of magnetospheric convection stratification, *Planet. Space Sci.*, *32*, 127.

Tung, Y.-K., C. W. Carlson, J. P. McFadden, D. M. Klumpar, G. K. Parks, W. J. Peria, and K. Liou (2001), Auroral polar cap boundary ion conic outflow observed on FAST, *J. Geophys. Res.*, *106*, 3603.

Volwerk, M., P. Louarn, T. Chust, A. Roux, A. de Fraudy, and B. Holback (1996), Solitary kinetic Alfvén waves: A study of the Poynting flux, *J. Geophys. Res.*, *101*, 13,335.

Vondrak, R. R. (1981), Chatanika radar measurements of the electrical properties of auroral arcs, in *Physics of Auroral Arc Formation*, *Geophys. Monogr. Ser.*, vol. 25, edited by S.-I. Akasofu and J. R. Kan, p. 185, AGU, Washington, D.C.

Wu, K., and C. E. Seyler (2003), Instability of inertial Alfven waves in transverse sheared flow, *J. Geophys. Res.*, *108*(A6), 1236, doi:10.1029/2002JA009631.

J. W. Bonnell, C. W. Carlson, C. C. Chaston, and J. P. McFadden, Space Sciences Laboratory, University of California, Berkeley, Centennial Drive at Grizzly Peak Blvd., Berkeley, CA 94720-7450, USA. (jbonnell@ssl.berkeley.edu; cwc@ssl.berkeley.edu; ccc@ssl.berkeley.edu; mcfadden@ssl.berkeley.edu)

R. E. Ergun, Laboratory for Atmospheric and Terrestrial Physics, University of Colorado, Boulder, CO 80303, USA. (ree@fast.boulder.edu)

E. J. Lund, Space Science Center, University of New Hampshire, Durham, NH 03824, USA. (lund@cluster1.sr.unh.edu)

R. J. Strangeway, Institute for Geophysical and Planetary Physics, University of California, Los Angeles, CA 90024, USA. (strange@igpp.ucla.edu)